Supporting Information

Effect of Pore Size, Solvation and Defectivity on the Perturbation of Adsorbates in MOFs: the Paradigmatic Mg_2(dobpdc) Case Study

Jenny G. Vitillo,[‡†]* Gabriele Ricchiardi[†]

[†]Department of Chemistry, NIS Centre and INSTM, University of Turin, via Quarello 15, I-10135 Torino, Italy.
[‡]Department of Chemistry, University of Minnesota, 207 Pleasant Street S.E., Minneapolis, MN 55455-0431. Phone: 612-624-5923. E-mail: jg.vitillo@gmail.com.

Content

S1. Materials and methods 2

S2. Optimised structures of Mg_2(dobpdc)–*act*, CO_2/Mg_2(dobpdc)–*act*, CO/Mg_2(dobpdc)–*act* and N_2/Mg_2(dobpdc)–*act*. 3

S3. ATR-FTIR spectrum of Mg_2(dobpdc)–*act* 12

S4. IR spectra of toluene, chloroform, methanol, and water on Mg_2(dobpdc)–*act*. 16

S5. Volumetric measurements of N_2 at 77 K and CO_2 at RT. 24

S6. IR spectra of CO_2 on Mg_2(dobpdc)–*act*, on Mg_2(dobpdc)–*sol* and Mg_2(dobpdc)–*air*. 26

S7. IR spectra of CO at 100 K on Mg_2(dobpdc)–*act*, Mg_2(dobpdc)–*sol* and Mg_2(dobpdc)–*air*. . 29

S8. IR spectra of N_2 at 100 K on Mg_2(dobpdc)–*act*, on Mg_2(dobpdc)–*sol* and Mg_2(dobpdc)–*air*. 32

S9. Electrostatic potential maps of MOF-74-Mg and Mg_2(dobpdc)–*act* 35

S10. Instructions to visualize the calculated vibrational modes of Mg_2(dobpdc)–*act*, CO_2/Mg_2(dobpdc)–*act*, CO/Mg_2(dobpdc)–*act* and N_2/Mg_2(dobpdc)–*act*. 37

S1. Materials and methods

FTIR spectroscopy in attenuated total reflection (ATR-FTIR). Fourier transformed infrared spectra in air (2 cm^{-1} resolution, average on 256 scans) were collected in Attenuated Total Reflection (ATR) mode on loose powder on a Bruker Alpha spectrophotometer (DTGS detector), equipped with an internal reflection element in diamond and placed in a M Braun Lab Star Glove Box supplied with pure 5.5 grade Nitrogen (<0.5 ppm O_2, <0.5 ppm H_2O). The relative intensity of the bands over the spectral region considered was corrected for the different decay in the sample of the evanescent wave as function of the incident wavelength, by dividing the original band intensities by the corresponding absorption wavelength.

S2. Optimised structures of Mg_2(dobpdc)–*act*, CO_2/Mg_2(dobpdc)–*act*, CO/Mg_2(dobpdc)–*act* and N_2/Mg_2(dobpdc)–*act*.

The inclusion of the Grimme correction caused a shrinking of the cell volume of about 2% and a shortening of the average Mg-O bond length from 2.052 to 2.040 Å. The calculated cell parameters after the inclusion in the Hamiltonian of the D* terms become closer to their experimental values ($a = b$ = 21.7008(8) Å and c = 6.847 (1) Å)[1] being the calculated values 0.8/2% and 0.5/0.9% larger than their experimental values before and after the Grimme correction. The IR spectra calculated for Mg_2(dobpdc) with and without the Grimme correction are reported in Figure S2, showing that the inclusion of the Grimme correction has only a slight influence on the intensity of some peaks.

Basis sets used

```
1 4
0 0 3 1.0 1.00
  34.0613410          0.602519780E-02
   5.12357460          0.450210940E-01
   1.16466260          0.201897260
0 0 1 0.0 1.00
   0.327230410           1.00000000
0 0 1 0.0 1.00
   0.103072410           1.00000000
0 2 1 0.00 1.00
   0.8000000000D+00  0.1000000000D+01
6 10
0 0 5 2.0 1.00
  8506.03840          0.533736640E-03
  1275.73290          0.412502320E-02
   290.311870          0.211713370E-01
    82.0562000          0.824178600E-01
    26.4796410          0.240128580
0 0 1 2.0 1.00
     9.24145850           1.00000000
0 0 1 0.0 1.00
     3.36435300           1.00000000
0 0 1 0.0 1.00
     0.871741640           1.00000000
```

```
0 0 1 0.0 1.00
     0.363523520          1.00000000
0 0 1 0.0 1.00
     0.128731350          1.00000000
0 2 4 2.0 1.00
    34.7094960         0.533009740E-02
     7.95908830         0.358658140E-01
     2.37869720         0.142002990
     0.815400650         0.342031050
0 2 1 0.0 1.00
     0.289537850          1.00000000
0 2 1 0.0 1.00
     0.100847540          1.00000000
0 3 1 0.00 1.00
     0.8000000000D+00  0.1000000000D+01
107 10
0 0 5 2.0 1.00
       11913.4168        -0.522970174E-03
       1786.72138        -0.404284040E-02
       406.590128        -0.207727151E-01
       114.925251        -0.811831378E-01
       37.1058834        -0.238714974
0 0 1 2.0 1.00
       12.9716762          1.00000000
0 0 1 0.0 1.00
       4.73022912          1.00000000
0 0 1 0.0 1.00
       1.25251843          1.00000000
0 0 1 0.0 1.00
      0.512600712          1.00000000
0 0 1 0.0 1.00
      0.179397140          1.00000000
0 2 4 3.0 1.00
       49.2187584         0.555269535E-02
       11.3489353         0.380546180E-01
       3.42850882         0.149414122
       1.17995126         0.348981874
0 2 1 0.0 1.00
      0.417261226          1.00000000
0 2 1 0.0 1.00
      0.142951313          1.00000000
0 3 1 0.00 1.00
      0.1000000000D+01  0.1000000000D+01
8 10
0 0 5 2.0 1.00
 15902.6475         0.514998037E-03
  2384.95378         0.398197644E-02
   542.719572         0.204769719E-01
   153.404079         0.802623679E-01
    49.5457161         0.237668399
0 0 1 2.0 1.00
    17.3396499          1.00000000
0 0 1 0.0 1.00
     6.33033553          1.00000000
```

```
0 0 1 0.0 1.00
     1.69958822          1.00000000
0 0 1 0.0 1.00
     0.689544913          1.00000000
0 0 1 0.0 1.00
     0.239360282          1.00000000
0 2 4 4.0 1.00
    63.2705240          0.607092060E-02
    14.6233123          0.419476887E-01
     4.44895180          0.161568840
     1.52815132          0.356827793
0 2 1 0.0 1.00
     0.529973159          1.00000000
0 2 1 0.0 1.00
     0.175094460          1.00000000
0 3 1 0.00 1.00
     0.1200000000D+01  0.1000000000D+01
12 8
0 0 7 2. 1.00
 31438.3496          0.609123113E-03
  4715.51534          0.470661965E-02
  1073.16292          0.241358207E-01
   303.572388          0.936289598E-01
    98.6262510          0.266467421
    34.9438084          0.478909299
    12.8597852          0.336984903
0 0 3 2. 1.00
    64.8769130          0.191808893E-01
    19.7255208          0.909137044E-01
     2.89518043         -0.395637561
0 0 2 2. 1.00
     1.19604547          1.68276034
     0.543294512         0.521410920
0 0 1 0. 1.00
     0.100991041          1.00000000
0 2 5 6. 1.00
   179.871896          0.537995490E-02
    42.1200694          0.393180141E-01
    13.1205030          0.157401295
     4.62575036          0.359190941
     1.66952110          0.455333793
0 2 1  0. 1.00
     0.585510121          1.00000000
0 2 1  0. 1.00
     0.189                1.00000000
0 3 1  0. 1.00
    3.444  1.00
108 10
0 0 5 2.0 1.00
 15902.6475          0.514998037E-03
  2384.95378          0.398197644E-02
   542.719572         0.204769719E-01
   153.404079         0.802623679E-01
    49.5457161         0.237668399
```

```
0 0 1 2.0 1.00
    17.3396499          1.00000000
0 0 1 0.0 1.00
     6.33033553          1.00000000
0 0 1 0.0 1.00
     1.69958822          1.00000000
0 0 1 0.0 1.00
     0.689544913          1.00000000
0 0 1 0.0 1.00
     0.239360282          1.00000000
0 2 4 4.0 1.00
    63.2705240          0.607092060E-02
    14.6233123          0.419476887E-01
     4.44895180          0.161568840
     1.52815132          0.356827793
0 2 1 0.0 1.00
     0.529973159          1.00000000
0 2 1 0.0 1.00
     0.175094460          1.00000000
0 3 1 0.00 1.00
     0.1200000000D+01  0.1000000000D+01
106 10
0 0 5 2.0 1.00
  8506.03840          0.533736640E-03
  1275.73290          0.412502320E-02
   290.311870          0.211713370E-01
    82.0562000          0.824178600E-01
    26.4796410          0.240128580
0 0 1 2.0 1.00
     9.24145850          1.00000000
0 0 1 0.0 1.00
     3.36435300          1.00000000
0 0 1 0.0 1.00
     0.871741640          1.00000000
0 0 1 0.0 1.00
     0.363523520          1.00000000
0 0 1 0.0 1.00
     0.128731350          1.00000000
0 2 4 2.0 1.00
    34.7094960          0.533009740E-02
     7.95908830          0.358658140E-01
     2.37869720          0.142002990
     0.815400650          0.342031050
0 2 1 0.0 1.00
     0.289537850          1.00000000
0 2 1 0.0 1.00
     0.100847540          1.00000000
0 3 1 0.00 1.00
     0.8000000000D+00  0.1000000000D+01
```

Structure of Mg_2(dobpdc)–*act* as optimized at the B3LYP/TZVp level (CIF file format):

```
data_-
_audit_creation_date              26-09-2016
_audit_creation_method            'crystal14 opt'
_symmetry_space_group_name_H-M    'P3221'
_symmetry_Int_Tables_number       154
_symmetry_cell_setting            HEXAGONAL
loop_
_symmetry_equiv_pos_as_xyz
  x,y,z
  -y,x-y,z+2/3
  -x+y,-x,z+1/3
  y,x,-z
  x-y,-y,-z+1/3
  -x,-x+y,-z+2/3
_cell_length_a                    21.86973288
_cell_length_b                    21.86973288
_cell_length_c                    6.98686837
_cell_angle_alpha                 90.000000
_cell_angle_beta                  90.000000
_cell_angle_gamma                 120.000000
loop_
_atom_site_label
_atom_site_type_symbol
_atom_site_fract_x
_atom_site_fract_y
_atom_site_fract_z
_atom_site_U_iso_or_equiv
_atom_site_adp_type
_atom_site_occupancy
MG1 MG -3.806877655510E-01 2.845434708402E-01 1.529850449467E-01 0.00000  Uiso   1.00
O7 O -3.500571700737E-01 2.394379411321E-01 -5.330923148472E-02 0.00000  Uiso   1.00
O13 O -3.581389483949E-01 3.559863783848E-01 -7.056418553113E-02 0.00000  Uiso   1.00
O19 O -4.147830531929E-01 2.099275713151E-01 3.648848502020E-01 0.00000  Uiso   1.00
C25 C -3.842043228117E-01 1.757692446033E-01 -1.365439330723E-01 0.00000  Uiso   1.00
C31 C -4.298344279646E-01 4.060474368230E-01 1.533840373859E-03 0.00000  Uiso   1.00
C37 C -4.629786851675E-01 4.421535587591E-01 -7.020393755721E-02 0.00000  Uiso   1.00
H43 H -4.519724548539E-01 4.595187976372E-01 -2.175139368431E-01 0.00000  Uiso   1.00
C49 C 4.929655725960E-01 4.567104056376E-01 4.015115841648E-02 0.00000  Uiso   1.00
C55 C -4.342549177860E-01 4.886623794256E-02 -1.015267412609E-01 0.00000  Uiso   1.00
H61 H -4.431080653452E-01 4.907011082718E-03 -1.132118375469E-02 0.00000  Uiso   1.00
C67 C -3.996891579206E-01 1.161115770805E-01 -2.571361436713E-02 0.00000  Uiso   1.00
H73 H -3.826576617026E-01 1.248982197002E-01 1.221035395643E-01 0.00000  Uiso   1.00
C79 C -3.852907329715E-01 3.924804038048E-01 -1.318391505482E-01 0.00000  Uiso   1.00
```

Structure of Mg_2(dobpdc)–*act* as optimized at the B3LYP-D*/TZVp level (CIF file format):

```
data_-
_audit_creation_date              20-11-2016
_audit_creation_method            'crystal14 opt from J.G. Vitillo crytocif script'
_symmetry_space_group_name_H-M    'P3221'
_symmetry_Int_Tables_number       154
_symmetry_cell_setting            HEXAGONAL
loop_
_symmetry_equiv_pos_as_xyz
  x,y,z
  -y,x-y,z+2/3
  -x+y,-x,z+1/3
  y,x,-z
  x-y,-y,-z+1/3
  -x,-x+y,-z+2/3
_cell_length_a                    21.81334463
_cell_length_b                    21.81334463
_cell_length_c                    6.90818840
_cell_angle_alpha                 90.000000
_cell_angle_beta                  90.000000
_cell_angle_gamma                 120.000000
loop_
_atom_site_label
_atom_site_type_symbol
_atom_site_fract_x
_atom_site_fract_y
_atom_site_fract_z
_atom_site_U_iso_or_equiv
_atom_site_adp_type
```

```
_atom_site_occupancy
MG1 MG -3.811560911139E-01 2.841271944372E-01 1.524411575762E-01 0.00000  Uiso   1.00
O7 O -3.480919576095E-01 2.397337829440E-01 -5.000387429958E-02 0.00000  Uiso   1.00
O13 O -3.592249172517E-01 3.545953996226E-01 -7.218528798081E-02 0.00000  Uiso   1.00
O19 O -4.149606909544E-01 2.094398649947E-01 3.637359092785E-01 0.00000  Uiso   1.00
C25 C -3.829050435402E-01 1.758616455377E-01 -1.331601042264E-01 0.00000  Uiso   1.00
C31 C -4.307168198618E-01 4.049918970620E-01 3.035141007335E-03 0.00000  Uiso   1.00
C37 C -4.637727668903E-01 4.412407452674E-01 -6.979334203501E-02 0.00000  Uiso   1.00
H43 H -4.525555168848E-01 4.587043884170E-01 -2.186416517397E-01 0.00000  Uiso   1.00
C49 C 4.918973503667E-01 4.556798022882E-01 4.121134067969E-02 0.00000  Uiso   1.00
C55 C -4.334184682577E-01 4.865698286481E-02 -9.791972917319E-02 0.00000  Uiso   1.00
H61 H -4.423965080866E-01 4.519046227380E-03 -6.832955312489E-03 0.00000  Uiso   1.00
C67 C -3.988531713111E-01 1.160117255540E-01 -2.072743349704E-02 0.00000  Uiso   1.00
H73 H -3.819562793406E-01 1.247752429734E-01 1.289087033956E-01 0.00000  Uiso   1.00
C79 C -3.860454885198E-01 3.917321569441E-01 -1.320404415919E-01 0.00000  Uiso   1.00
```

Structure of CO_2/Mg_2(dobpdc)–*act* ($P3_2$ symmetry, no imaginary frequency) as optimized at the B3LYP-D*/TZVp level (CIF file format):

```
data_-
_audit_creation_date              13-12-2016
_audit_creation_method            'crystal14 opt from J.G. Vitillo crytocif script'
_symmetry_space_group_name_H-M    'P32'
_symmetry_Int_Tables_number       145
_symmetry_cell_setting            trigonal
loop_
_symmetry_equiv_pos_as_xyz
  x,y,z
  -y,x-y,z+2/3
  -x+y,-x,z+1/3
_cell_length_a                    21.65485370
_cell_length_b                    21.65485370
_cell_length_c                    6.91610509
_cell_angle_alpha                 90.000000
_cell_angle_beta                  90.000000
_cell_angle_gamma                 120.000000
loop_
_atom_site_label
_atom_site_type_symbol
_atom_site_fract_x
_atom_site_fract_y
_atom_site_fract_z
_atom_site_U_iso_or_equiv
_atom_site_adp_type
_atom_site_occupancy
MG1 MG -3.812742505293E-01 2.807066655199E-01 1.383717106102E-01 0.00000  Uiso   1.00
MG4 MG 3.380810993408E-01 -2.806535222879E-01 1.899210192062E-01 0.00000  Uiso   1.00
O7 O -3.391883536029E-01 2.422171094366E-01 -5.915115631780E-02 0.00000  Uiso   1.00
O10 O 4.188271419488E-01 -2.424014195250E-01 3.876372384654E-01 0.00000  Uiso   1.00
O13 O -3.596635168450E-01 3.537076145819E-01 -7.985691138792E-02 0.00000  Uiso   1.00
O16 O 2.866474329837E-01 -3.532131861122E-01 4.086738454744E-01 0.00000  Uiso   1.00
O19 O -4.083380388758E-01 2.073148077114E-01 3.559550061000E-01 0.00000  Uiso   1.00
O22 O 3.853859282150E-01 -2.072859356520E-01 -2.700194969488E-02 0.00000  Uiso   1.00
C25 C -3.717223734628E-01 1.780757179671E-01 -1.413820859634E-01 0.00000  Uiso   1.00
C28 C 4.505598165147E-01 -1.782540124191E-01 4.696902447093E-01 0.00000  Uiso   1.00
C31 C -4.402351188054E-01 3.946387550998E-01 -4.365281550883E-03 0.00000  Uiso   1.00
C34 C 1.651918856612E-01 -3.939988596268E-01 3.327711373682E-01 0.00000  Uiso   1.00
C37 C -4.759041716876E-01 4.290328499312E-01 -7.546469234495E-02 0.00000  Uiso   1.00
C40 C 9.505963150107E-02 -4.286081370799E-01 4.032904204647E-01 0.00000  Uiso   1.00
H43 H -4.651427167189E-01 4.473002148257E-01 -2.236569487704E-01 0.00000  Uiso   1.00
H46 H 8.741905676699E-02 -4.468073504914E-01 -4.484582934914E-01 0.00000  Uiso   1.00
C49 C 4.783570882399E-01 4.416538535996E-01 3.674094906812E-02 0.00000  Uiso   1.00
C52 C 3.668574391463E-02 -4.416140747412E-01 2.905027695605E-01 0.00000  Uiso   1.00
C55 C -4.184709427285E-01 5.043386420183E-02 -1.033197911462E-01 0.00000  Uiso   1.00
C58 C -4.691659955647E-01 -5.050207112654E-02 4.304405857059E-01 0.00000  Uiso   1.00
H61 H -4.258854228769E-01 6.706562944560E-03 -1.150002647946E-02 0.00000  Uiso   1.00
H64 H -4.333330597084E-01 -6.787368856782E-03 3.378828151259E-01 0.00000  Uiso   1.00
C67 C -3.851082359665E-01 1.185993917122E-01 -2.816719347695E-02 0.00000  Uiso   1.00
C70 C 4.962414797925E-01 -1.187821191186E-01 3.558944164133E-01 0.00000  Uiso   1.00
H73 H -3.674902151810E-01 1.284953632425E-01 1.208371810945E-01 0.00000  Uiso   1.00
H76 H -4.962067585383E-01 -1.288083869257E-01 2.068756553637E-01 0.00000  Uiso   1.00
C79 C -3.922452096709E-01 3.855582104685E-01 -1.393914032988E-01 0.00000  Uiso   1.00
C82 C 2.222188133386E-01 -3.847967934524E-01 4.681994244205E-01 0.00000  Uiso   1.00
```

```
O85 O -4.948205980047E-01 1.977706609910E-01 3.909056878302E-02 0.00000  Uiso   1.00
O88 O 3.111625230029E-01 -1.949236641562E-01 2.920867261294E-01 0.00000  Uiso   1.00
C91 C 4.665100353462E-01 1.462059125031E-01 1.249109534680E-01 0.00000  Uiso   1.00
C94 C 3.356085488560E-01 -1.380080512923E-01 2.244597799855E-01 0.00000  Uiso   1.00
O97 O -3.317783200806E-01 -4.269418660008E-01 -4.601463047775E-01 0.00000  Uiso   1.00
O100 O 8.165528556793E-02 4.400226996875E-01 -1.730178839646E-01 0.00000  Uiso   1.00
```

Structure of CO_2/Mg_2(dobpdc)–*act* ($P3_221$ symmetry, 5 imaginary frequencies) as optimized at the B3LYP-D*/TZVp level (CIF file format):

```
data_-
_audit_creation_date              26-10-2016
_audit_creation_method            'crystal14 opt from J.G. Vitillo crytocif script'
_symmetry_space_group_name_H-M    'P3221'
_symmetry_Int_Tables_number       154
_symmetry_cell_setting            HEXAGONAL
loop_
_symmetry_equiv_pos_as_xyz
  x,y,z
  -y,x-y,z+2/3
  -x+y,-x,z+1/3
  y,x,-z
  x-y,-y,-z+1/3
  -x,-x+y,-z+2/3
_cell_length_a                    21.77399557
_cell_length_b                    21.77399557
_cell_length_c                    6.93220481
_cell_angle_alpha                 90.000000
_cell_angle_beta                  90.000000
_cell_angle_gamma                 120.000000
loop_
_atom_site_label
_atom_site_type_symbol
_atom_site_fract_x
_atom_site_fract_y
_atom_site_fract_z
_atom_site_U_iso_or_equiv
_atom_site_adp_type
_atom_site_occupancy
MG1 MG -3.833574521223E-01 2.835047357602E-01 1.517288021432E-01 0.00000  Uiso   1.00
O7 O -3.495258339699E-01 2.389988194923E-01 -4.617699375976E-02 0.00000  Uiso   1.00
O13 O -3.537010468108E-01 3.593898213124E-01 -6.357445658315E-02 0.00000  Uiso   1.00
O19 O -4.179775155472E-01 2.102610334775E-01 3.706001609471E-01 0.00000  Uiso   1.00
C25 C -3.849195334512E-01 1.755600788140E-01 -1.299743420991E-01 0.00000  Uiso   1.00
C31 C -4.281775207009E-01 4.071593442522E-01 7.077339552055E-03 0.00000  Uiso   1.00
C37 C -4.613925587844E-01 4.431478458749E-01 -6.698422996051E-02 0.00000  Uiso   1.00
H43 H -4.499013060264E-01 4.605014285522E-01 -2.153996771693E-01 0.00000  Uiso   1.00
C49 C 4.938404201611E-01 4.576973459470E-01 4.204433167222E-02 0.00000  Uiso   1.00
C55 C -4.355981670180E-01 4.791638453140E-02 -9.754435235826E-02 0.00000  Uiso   1.00
H61 H -4.447768378179E-01 3.939281972221E-03 -7.790282687385E-03 0.00000  Uiso   1.00
C67 C -4.008731852326E-01 1.152024477920E-01 -1.941140763509E-02 0.00000  Uiso   1.00
H73 H -3.839083662069E-01 1.237280502823E-01 1.297731112749E-01 0.00000  Uiso   1.00
C79 C -3.819662539900E-01 3.947790364193E-01 -1.254175687489E-01 0.00000  Uiso   1.00
O85 O -4.998120246688E-01 2.201403594346E-01 5.482658318946E-02 0.00000  Uiso   1.00
C91 C 4.527028400301E-01 1.954341831824E-01 1.629530590313E-01 0.00000  Uiso   1.00
O97 O -2.342306646986E-01 -4.049943330657E-01 -3.998966596929E-01 0.00000  Uiso   1.00
```

Structure of CO/Mg_2(dobpdc)–*act* as optimized at the B3LYP-D*/TZVp level (CIF file format):

```
data_-
_audit_creation_date              12-10-2016
_audit_creation_method            'crystal14 opt'
_symmetry_space_group_name_H-M    'P3221'
_symmetry_Int_Tables_number       154
_symmetry_cell_setting            HEXAGONAL
loop_
_symmetry_equiv_pos_as_xyz
  x,y,z
  -y,x-y,z+2/3
```

```
  -x+y,-x,z+1/3
  y,x,-z
  x-y,-y,-z+1/3
  -x,-x+y,-z+2/3
_cell_length_a                    21.77116686
_cell_length_b                    21.77116686
_cell_length_c                    6.94787298
_cell_angle_alpha                 90.000000
_cell_angle_beta                  90.000000
_cell_angle_gamma                 120.000000
loop_
_atom_site_label
_atom_site_type_symbol
_atom_site_fract_x
_atom_site_fract_y
_atom_site_fract_z
_atom_site_U_iso_or_equiv
_atom_site_adp_type
_atom_site_occupancy
MG1 MG -3.835581641602E-01 2.830676839988E-01 1.510682663219E-01 0.00000  Uiso   1.00
O7 O -3.488814009294E-01 2.393281495009E-01 -4.852937931280E-02 0.00000  Uiso   1.00
O13 O -3.530471814196E-01 3.600689248982E-01 -6.412016526669E-02 0.00000  Uiso   1.00
O19 O -4.153351423152E-01 2.100042951292E-01 3.678427543569E-01 0.00000  Uiso   1.00
C25 C -3.841924122843E-01 1.758561928464E-01 -1.315571226591E-01 0.00000  Uiso   1.00
C31 C -4.290238552472E-01 4.062191735065E-01 5.614805323070E-03 0.00000  Uiso   1.00
C37 C -4.623413679862E-01 4.422282021532E-01 -6.785667117116E-02 0.00000  Uiso   1.00
H43 H -4.510802718950E-01 4.593794569992E-01 -2.161247498555E-01 0.00000  Uiso   1.00
C49 C 4.932770099009E-01 4.570798368414E-01 4.162759186590E-02 0.00000  Uiso   1.00
C55 C -4.353964969118E-01 4.815221337705E-02 -9.796625472982E-02 0.00000  Uiso   1.00
H61 H -4.448010751891E-01 3.675673583077E-03 -7.894760112898E-03 0.00000  Uiso   1.00
C67 C -4.007835805565E-01 1.154668420881E-01 -2.035132833960E-02 0.00000  Uiso   1.00
H73 H -3.841979360559E-01 1.240768390415E-01 1.287623384308E-01 0.00000  Uiso   1.00
C79 C -3.829491946406E-01 3.937984740811E-01 -1.275268519043E-01 0.00000  Uiso   1.00
C85 C 4.952014774075E-01 2.164443348975E-01 1.330200457866E-02 0.00000  Uiso   1.00
O91 O 4.393882787273E-01 1.867450247618E-01 -4.247674951845E-02 0.00000  Uiso   1.00
```

Structure of N_2/Mg_2(dobpdc)–*act* as optimized at the B3LYP-D*/TZVp level (CIF file format):

```
data_-
_audit_creation_date              24-10-2016
_audit_creation_method            'crystal14 opt'
_symmetry_space_group_name_H-M    'P3221'
_symmetry_Int_Tables_number       154
_symmetry_cell_setting            HEXAGONAL
loop_
_symmetry_equiv_pos_as_xyz
  x,y,z
  -y,x-y,z+2/3
  -x+y,-x,z+1/3
  y,x,-z
  x-y,-y,-z+1/3
  -x,-x+y,-z+2/3
_cell_length_a                    21.76999874
_cell_length_b                    21.76999874
_cell_length_c                    6.94168557
_cell_angle_alpha                 90.000000
_cell_angle_beta                  90.000000
_cell_angle_gamma                 120.000000
loop_
_atom_site_label
_atom_site_type_symbol
_atom_site_fract_x
_atom_site_fract_y
_atom_site_fract_z
_atom_site_U_iso_or_equiv
_atom_site_adp_type
_atom_site_occupancy
MG1 MG -3.829962821378E-01 2.834015737817E-01 1.523130470151E-01 0.00000  Uiso   1.00
O7 O -3.492403090124E-01 2.393702030157E-01 -4.849760734578E-02 0.00000  Uiso   1.00
O13 O -3.535449512575E-01 3.597136008399E-01 -6.414502395726E-02 0.00000  Uiso   1.00
O19 O -4.154892842885E-01 2.100470442168E-01 3.676747505422E-01 0.00000  Uiso   1.00
C25 C -3.842104277908E-01 1.758172268904E-01 -1.316962453799E-01 0.00000  Uiso   1.00
C31 C -4.290878817377E-01 4.062674354515E-01 5.410622367808E-03 0.00000  Uiso   1.00
C37 C -4.624395227817E-01 4.422210371200E-01 -6.814060487595E-02 0.00000  Uiso   1.00
H43 H -4.511147236297E-01 4.595819979128E-01 -2.163983384128E-01 0.00000  Uiso   1.00
C49 C 4.930506328155E-01 4.568485980877E-01 4.156374233375E-02 0.00000  Uiso   1.00
C55 C -4.350043349282E-01 4.821916722667E-02 -9.802635723199E-02 0.00000  Uiso   1.00
```

```
H61 H -4.443308669932E-01 3.764919709938E-03 -7.853864189770E-03 0.00000  Uiso   1.00
C67 C -4.004372031055E-01 1.155583134970E-01 -2.044314132072E-02 0.00000  Uiso   1.00
H73 H -3.837845026090E-01 1.242147453434E-01 1.287382418266E-01 0.00000  Uiso   1.00
C79 C -3.830969081922E-01 3.938074323287E-01 -1.276041329815E-01 0.00000  Uiso   1.00
N85 N 4.993855463268E-01 2.188822849234E-01 1.654841102768E-02 0.00000  Uiso   1.00
N91 N 4.455493348151E-01 1.899920067327E-01 -4.063272933261E-02 0.00000  Uiso   1.00
```

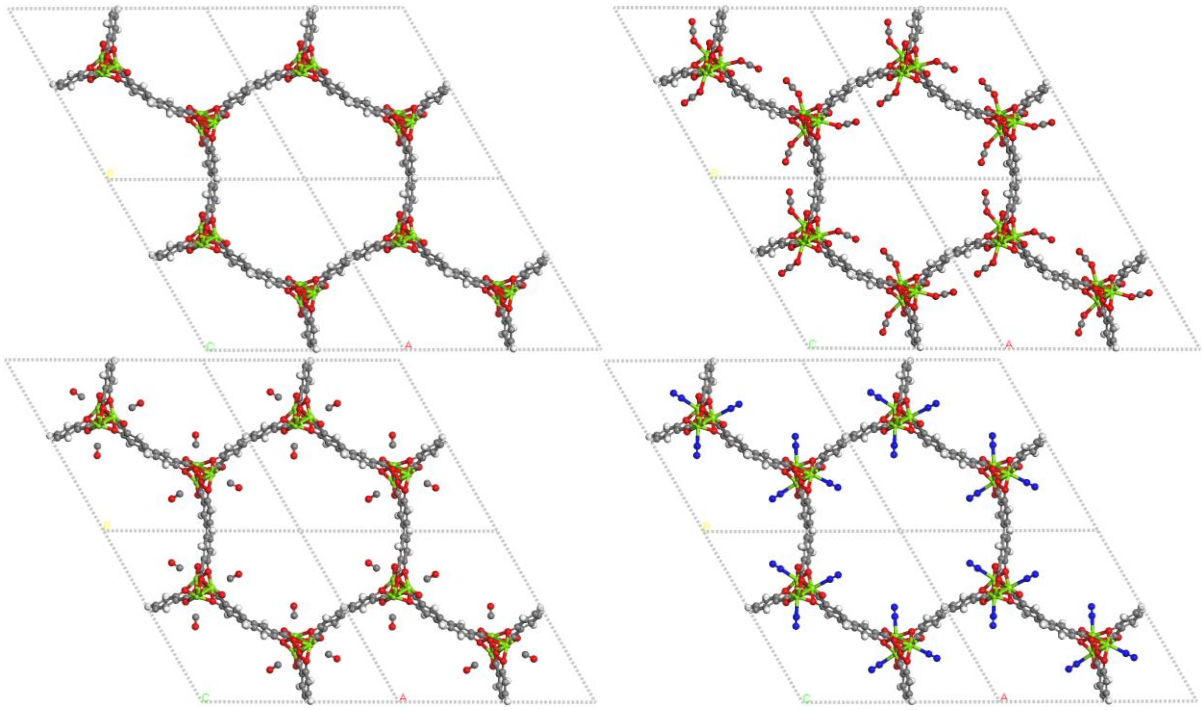

Figure S1. Optimized structures at B3-LYP-D*/TZVp of (from left to right, top to bottom) Mg_2(dobpdc)–*act*, CO_2/Mg_2(dobpdc)–*act*, CO/Mg_2(dobpdc)–*act* and N_2/Mg_2(dobpdc)–*act*. The C atoms are reported in gray, H atoms in white, O in red, Mg in green and N in blue.

S3. ATR-FTIR spectrum of Mg_2(dobpdc)–*act*

The ATR-IR spectrum of Mg_2(dobpdc)–*act* is shown in Figure S2. The corresponding spectrum as obtained in transmission is reported as red curve in Figure 1b of the article.

The IR spectra calculated for Mg_2(dobpdc) with and without the Grimme correction are also reported in Figure S1 as solid violet line and dotted magenta line, respectively, showing that the inclusion of the Grimme correction has only a slight influence on the intensity of some peaks. In both cases a good agreement with the experimental spectrum is obtained, although the calculated IR frequencies results shifted of +50 cm^{-1} with respect to the experimental ones.

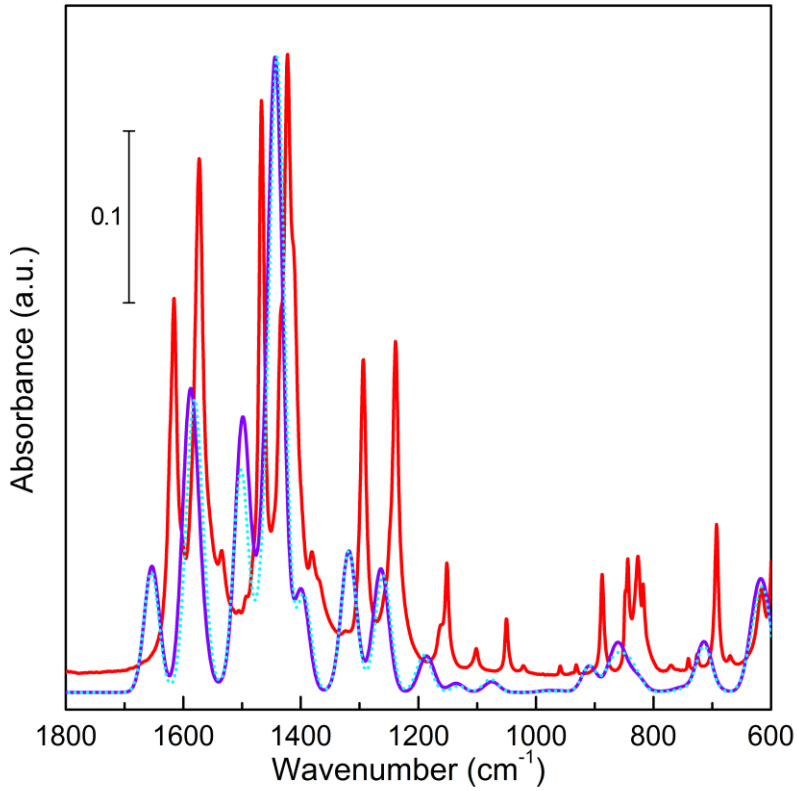

Figure S2. ATR-IR spectrum of Mg_2(dobpdc)–*act* in nitrogen atmosphere. Simulated IR spectra as obtained at the B3-LYP/TZVp level with (solid violet line) and without (dotted cyan line) the Grimme correction are also reported (Gaussian convolution, band width 30 cm^{-1}).

The assignment of the main IR bands presents in the spectrum of Mg_2(dobpdc)–*act* reported in Figure S2 on the basis of the calculations performed at the B3LYP-D*/TZVp level is shown in Table S1.

Table S1. Assignment of the IR vibrational modes of Mg_2(dobpdc)–*act* on the basis of periodic calculations performed at the B3LYP-D*/TZVp level.

Expt. frequency (cm^{-1})	Calc. IR mode (cm^{-1})	assignment
3066	3218-3212	ring beat mode
3034	3205-3187	C-H stretching
1616	1658-1652	asymmetric C-C stretching
1573	1597-1587	asymmetric COO stretching
1534	1580-1568	C-C stretching
1467	1532-1499	C-O (of alcohlate) stretching + C-H bending + ring stretching
1425	1478-1442	symmetric COO stretching + C-H bending + ring stretching
1384	1425-1398	symmetric COO stretching + C-H bending + ring stretching
1293	1343-1318	C-O (of alcohlate) stretching + symmetric C-C stretching of the two couples of vicinal C-H on the ring
	1293-1291	bending CCO (of alcoholate) + ring stretching
1239	1283-1263	C-O (of alcohlate) stretching + ring stretching
1160 (s) and 1151	1186-1173	CH bending (kekule)

1102	1136-1134	C(CH)C bending
1050	1075-1074	ring breathing
1021	519	overtone Mg-O stretching
958	983	C-H bending out of plane twisting
931	964-951	C-H bending out of plane
887	909-905	COO bending + CCC bend
844	871-865	C-H bending out of plane wagging
826	853-852	Mg-O stretching + ring breathing
818	828-823	C of COO movement out of plane + C-H bending out of plane
770	789	COO bending + CCC bending
741	758-743	COO bending + Ring torsion
726	758-743	COO bending + Ring torsion
693	718-714	COO bending + Ring deformation
669	684	CCC bending + Mg-O stretching
616	635	Mg-O stretching + ring rotation
	629-606	Mg-O stretching + CH out of plane wagging

S4. IR spectra of toluene, chloroform, methanol, and water on Mg_2(dobpdc)–*act*.

The IR spectra of toluene, chloroform, methanol, and water in interaction with Mg_2(dobpdc)–*act* at beam temperature are shown in Figure S3-Figure S7 at different gas pressures.

For toluene (Figure S3) and dichloromethane (Figure S4), being coincident the spectra recorded during adsorption and desorption, only the spectra obtained during adsorption have been reported. A significant perturbation of several MOF bands was observed upon solvent sorption (see Table S2).

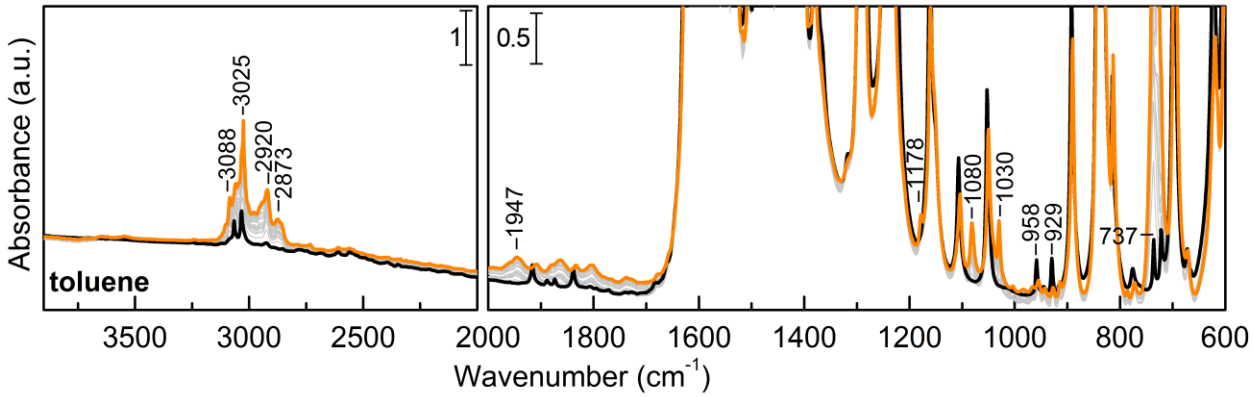

Figure S3. IR spectra of toluene at beam temperature on Mg_2(dobpdc)–*act*. The spectra are reported for increasing dosing of toluene from vacuum (black curve) up to 20 mbar (orange line). Light grey curves refer to intermediate coverage. The spectrum obtained after degassing overnight at beam temperature was coincident with that of Mg_2(dobpdc)–*act* and then it was not reported.

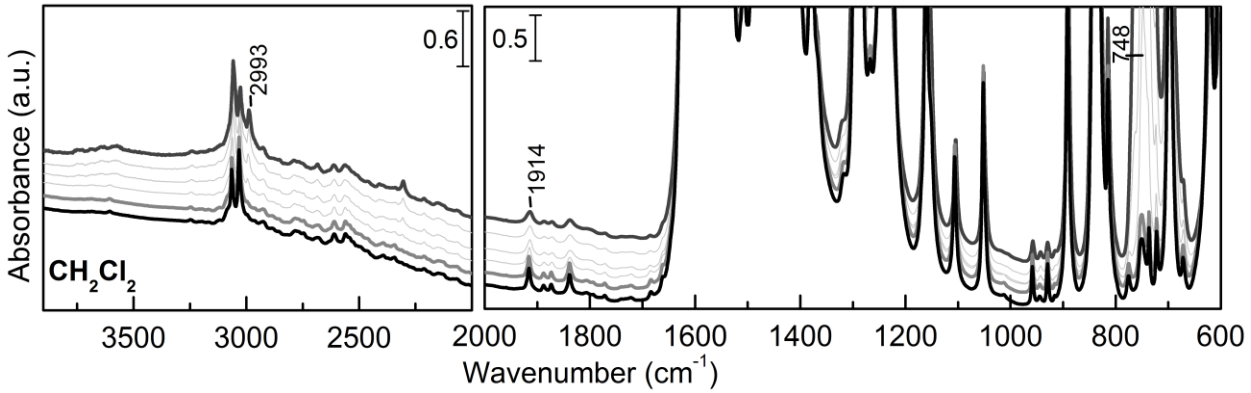

Figure S4. IR spectra of CH_2Cl_2 at beam temperature on Mg_2(dobpdc)–*act*. The spectra are reported for increasing dosing of CH_2Cl_2 from vacuum (black curve) up to 0.3 (grey curve) and 52 mbar (dark grey line). Light grey curves refer to intermediate coverage. The spectrum obtained after degassing overnight at beam temperature was coincident with that of Mg_2(dobpdc)–*act* and then it was not reported.

For methanol (Figure S5) and water (Figure S7), on the contrary, the spectra recorded during vapor adsorption and desorption have been plotted in two different graphs. These solvents were desorbed completely only at temperatures higher than BT, because of the strong interaction between the solvent molecules and Mg^{2+} ions. After prolonged degassing at beam temperature, only the solvent molecules bond to Mg^{2+} were left in the MOF, selectively poisoning these sites. For methanol, being the adsorption process characterized by a time evolution for pressures lower than 2 mbar, the spectra recorded in time for a pressure dose of 0.2 mbar are also reported in Figure S6 (see below for the discussion), evidencing as in this case the adsorption process is constituted by two steps. In the first step, methanol molecules form small clusters as suggested by the presence of the band at 3309 cm^{-1}. Slowly the clusters disaggregate with the migration of methanol molecules on the Mg^{2+} sites (band at 3603 cm^{-1}).

After outgassing overnight at 180°C the sample exposed to methanol, the initial spectrum was restored.

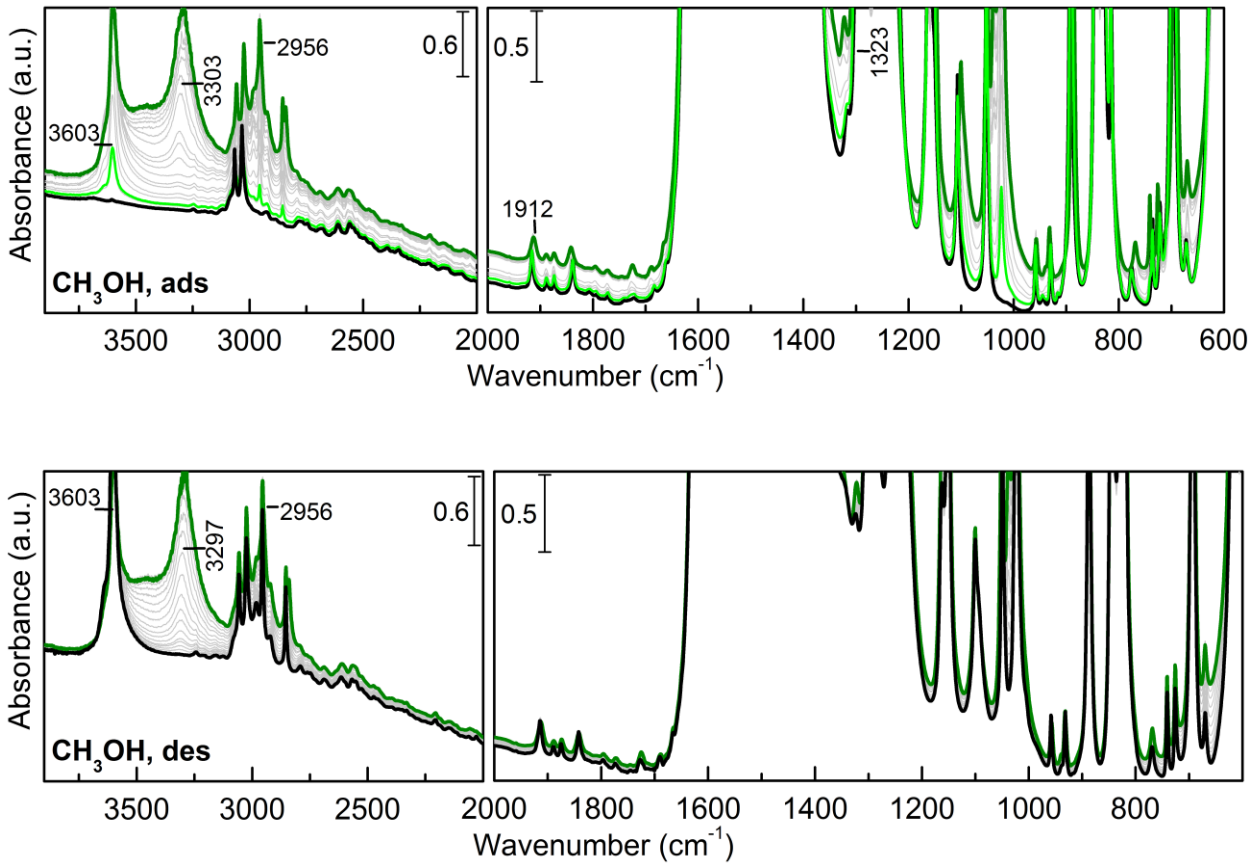

Figure S5. IR spectra of methanol at beam temperature on Mg_2(dobpdc)–*act*. (top) The spectra are reported for increasing dosing of CH_3OH from vacuum (black curve) to 0.7 mbar (dark green line) as obtained at equilibrium. The spectrum obtained at very low dosages is reported as light green line. Light grey curves refer to intermediate coverage. (bottom) The spectra are reported upon degassing at beam temperature. The spectrum obtained after degassing overnight at beam temperature is reported as black line. Light grey curves refer to intermediate coverage. The spectrum obtained after degassing overnight at 180°C was coincident with that of Mg_2(dobpdc)–*act* and then it was not reported.

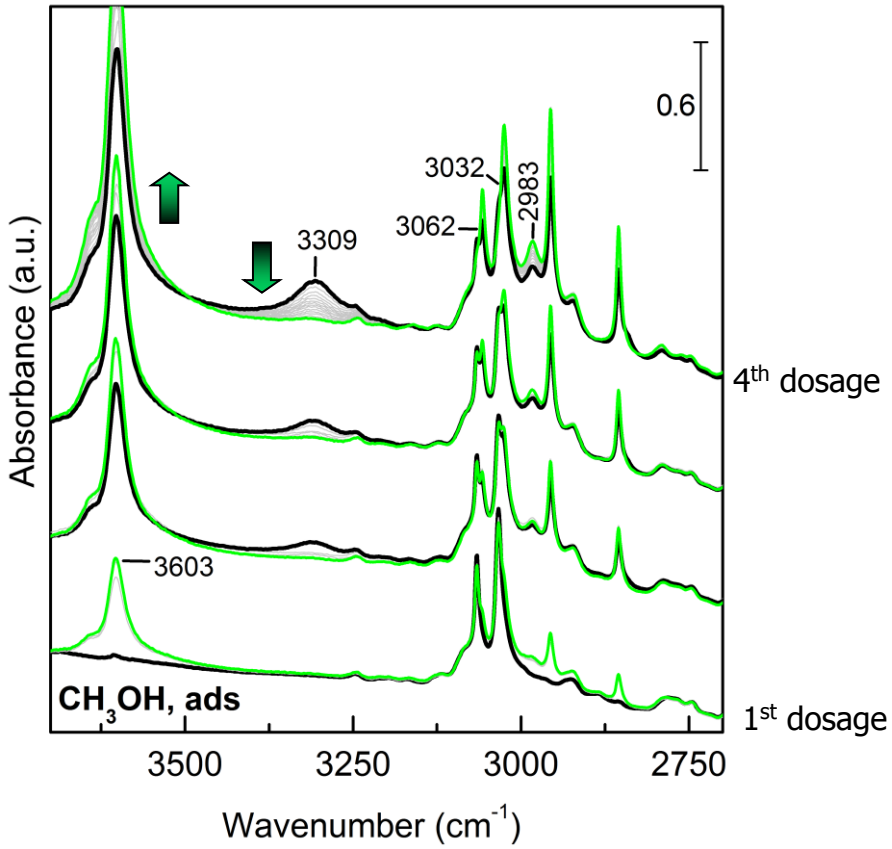

Figure S6. IR spectra of methanol at beam temperature on Mg_2(dobpdc)–*act* recorded in time upon subsequent dosages having a starting pressure of 0.2 mbar (from bottom to the top). Black spectra refer to the spectrum recorded immediately after the vapour dosage. Green spectra refer to spectra recorded at the equilibrium. Light grey curves refer to intermediate coverage. The disappearance of the band at 3309 cm^{-1} is evident with the parallel growth in intensity of the signal at 3603 cm^{-1}. The presence of two isosbestic points at 3062 and 3032 cm^{-1} marks the transition from methanol clusters to single methanol molecules adsorbed on Mg^{2+} sites.

In the case of water, on the contrary, after activation the MOF spectrum was characterized by the appearance of two signals in the OH region, related to the formation of defects. It is interesting to notice that no other significant changes were observed in the MOF spectrum, although the significant decrease in the material surface area (see Table S3 and Ref. 1).

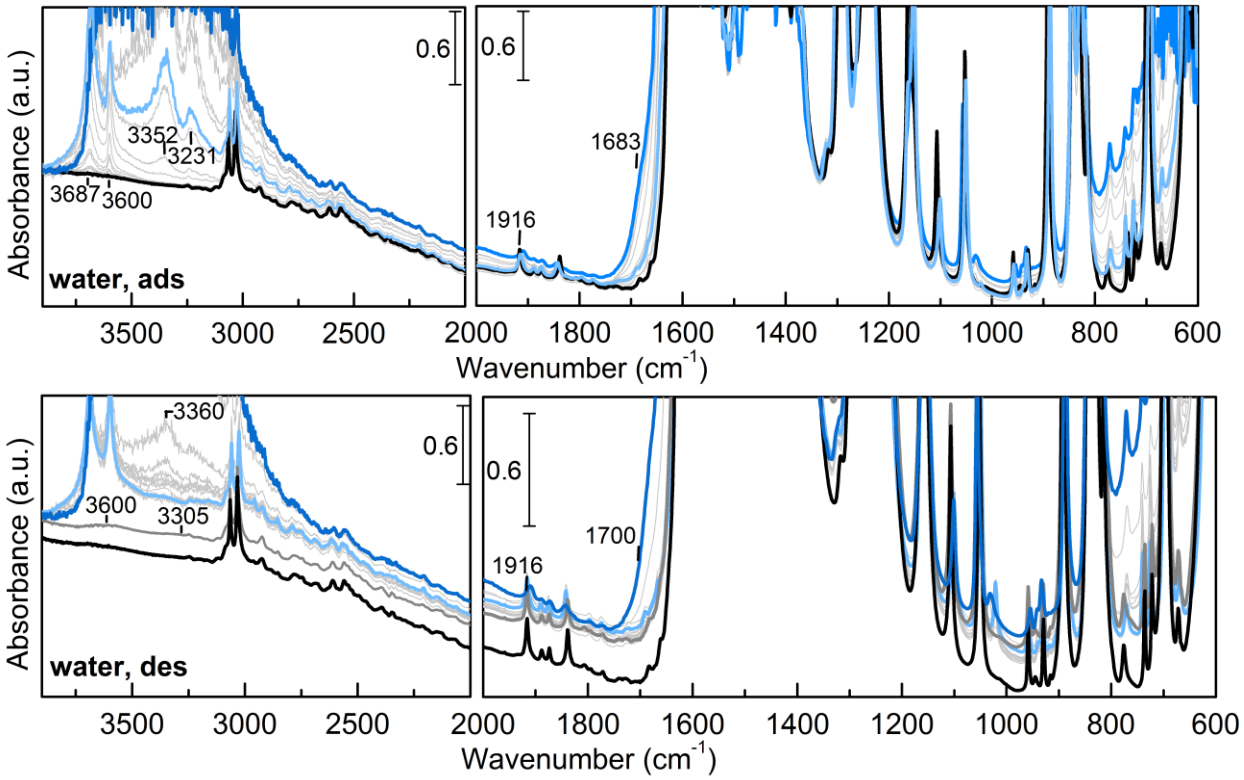

Figure S7. IR spectra of water at beam temperature on Mg_2(dobpdc)–*act*. (top) The spectra are reported for increasing dosing of H_2O from vacuum (black curve), to 1 (light blue curve) and 20 mbar (blue curve). Light grey curves refer to intermediate coverage. (bottom) The spectra are reported upon degassing at beam temperature. The spectrum obtained after degassing overnight at beam temperature is reported as light blue curve. Light grey curves refer to intermediate coverage. The spectrum obtained after degassing overnight at 250°C is reported as dark grey line.

The nature of these defects, that is of vicinal Mg-OH and HO-C couples (accordingly to what suggested in the literature),[2] allows to expect a partial restoration of exposed Mg^{2+} sites from condensation of vicinal hydroxyl groups as it happens on oxidic surfaces. A decrease in the signals related to –OH groups involved in H-bonds (3288 cm^{-1} band) is observed upon thermal treatment at increasing temperature by means of IR spectroscopy, validating this hypothesis (see Figure S8).

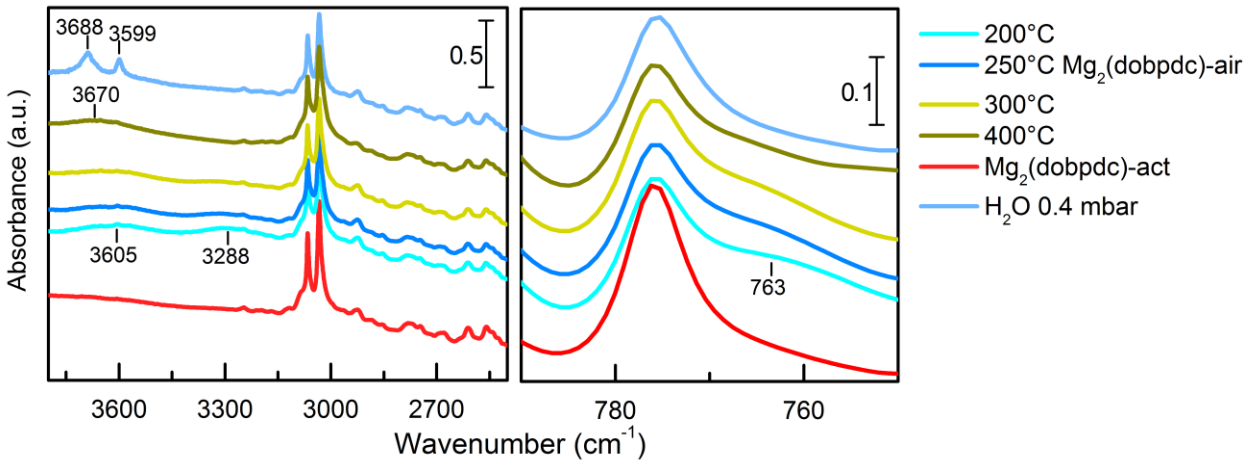

Figure S8. IR spectra obtained after activation at increasing temperatures of Mg_2(dobpdc)–*act* after exposure to a water saturated atmosphere. The spectrum of the undamaged Mg_2(dobpdc)–*act* sample is reported. The spectrum obtained after a dosage of water lower than the one necessary for the saturation of Mg^{2+} sites is also shown for comparison.

It is evident that no signal related to water molecules is present in these spectra at 200°C. The signals relative to hydroxyl groups (3605, 3288 and 763 cm^{-1}) decrease in intensity from 200 to 300°C. After treatment at 400°C, the band at 3288 cm^{-1} is disappeared suggesting the absence of vicinal hydroxyl groups whereas the band at 3605 cm^{-1}, relative to isolated hydroxyl groups, is shifted to higher wavenumbers (3670 cm^{-1}) suggesting the formation of more basic –OH and then to the formation of Mg-OH nanoclusters.

It has been previously reported that MOF decomposition can be avoided after material exposure to water if washed with acetone or a low surface tension solvent before pumping them down.[3] Although such an experiment cannot be carried out in the present apparatus, it would be interesting to verify if also for such an air-instable MOF, actually the decomposition happens during the water removal process. This issue will be addressed in future studies.

Table S2. Shift of IR vibrational modes of Mg_2(dobpdc)–*act* (in cm^{-1}) after interaction with different solvents at the higher vapor pressure considered (see Figures S3-S7).

mode	toluene	dichloromethane	methanol	water
1916	+31	-2	-4	-7
1838	+25	+1	+3	+4
1107	-3	-2	-7	-6
1053	-3	-2	-3	+3
958	-3	-1	-2	-4
929	-2	0	+3	+3
776	-4	–	-7	-5

S4.1 Time evolution of the solvents adsorption spectra

Besides the reversibility of the adsorption process, solvent polarity influenced also the time evolution of the adsorption process. In fact, for toluene and dichlorometane (that is for the solvents having the lowest polarity) the time evolution of the IR spectra after each vapor dosage was characterized by a parallel increase of the intensity of all the solvent bands until equilibration was reached. In the case of methanol, different behaviors were observed at different pressures.

At pressures lower than 1 mbar, after each pressure step a slow evolution is observed. Initially, methanol prefers to interact with other methanol molecules through hydrogen bonding (band at 3309 cm^{-1}) instead to coordinate to the MOF (peak at 3603 cm^{-1}). Only in a second time, they slowly migrate on the Mg^{2+} sites. The process can be easily followed in time by means of IR spectroscopy, showing the decrease in the intensity of the 3309 cm^{-1} signal and the parallel increase

of that located at 3603 cm^{-1} at each pressure pulse. In a qualitative description of the process, on the basis of the partial information obtained from the IR spectra, firstly the methanol molecules interact with the MOF walls preferentially through the methyl group leaving the -OH free to interact by hydrogen bonding with other methanol molecules forming small aggregates likely outside the pores. The slow diffusion of aggregates in the MOF pores and their interaction with an open Mg^{2+} site would cause the transfer of one methanol molecule from methanol clusters to the metal sites. At equilibrium, all the methanol molecules are coordinated to a Mg^{2+} site. At pressures higher than 1 mbar (even in the case of the first pressure dosage), this first step is not observed and coordination to Mg^{2+} occurs from the beginning. For what concerns water, such a process was not observed likely because of the strong polar nature of this molecule and its higher interaction energy with the Mg^{2+} sites.

S5. Volumetric measurements of N_2 at 77 K and CO_2 at RT.

The experimental N_2 isotherms obtained at 77 K on Mg_2(dobpdc)–*act*, Mg_2(dobpdc)–*sol* and Mg_2(dobpdc)–*air* are shown in Figure S9. The surface area and pore volume obtained from the analysis of these isotherms are reported in Table S3, along with the N_2 (at 77 K and 0.95 bar) and CO_2 (at RT and 1 bar) uptake. The values reported for MOF-74-Mg in Ref. [4] are also shown in this table. The comparison between MOF-74-Mg and Mg_2(dobpdc)–*act* evidences once again the important role of Mg^{2+} in the CO_2 adsorption in the pressure and temperature conditions adopted in the present paper: in fact, although MOF-74 is characterized by a surface area that is about half of the Mg_2(dobpdc)-act one, the CO_2 adsorbed per Mg^{2+} site is the same (about 1) and the CO_2 uptake per gram of material in even higher. This is due to the lower molecular mass of MOF-74-Mg formula unit.

For what concerns Mg_2(dobpdc)–*sol* and Mg_2(dobpdc)–*air*, it is impressive the larger detrimental effect on the CO_2 uptake of the poisoning of the Mg^{2+} sites by residual solvent molecules with respect to the degradation of the material, reversing what expected on the basis of the surface area measurements.

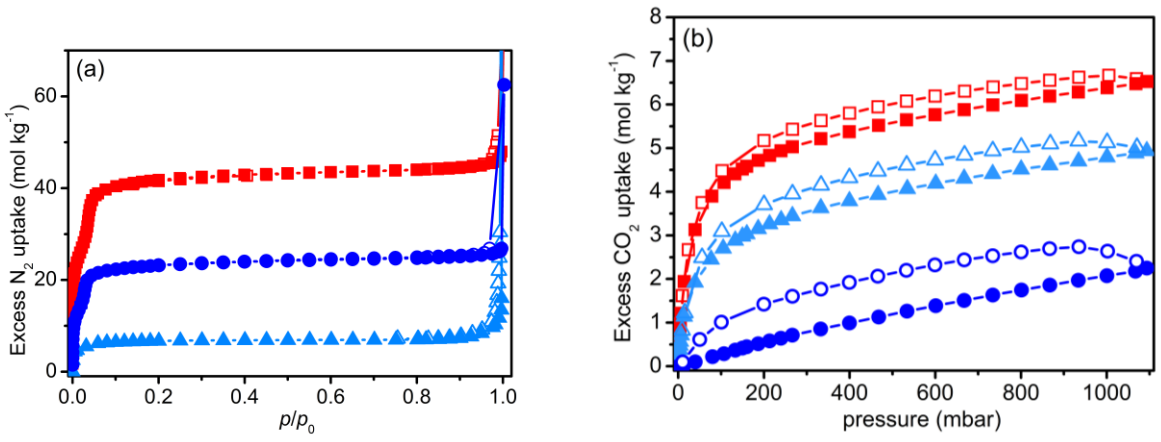

Figure S9. (a) N_2 isotherms at 77 K and (b) CO_2 isotherms at RT on Mg_2(dobpdc)–*act* (squares, red line), Mg_2(dobpdc)–*sol* (circles, blue line) and Mg_2(dobpdc)–*air* (triangles, light blue line). The full and empty scatters refer to the adsorption and desorption branches, respectively.

Table S3. Experimental Langmuir and BET surface area and pore volume for Mg_2(dobpdc)–*act*, Mg_2(dobpdc)–*sol*, Mg_2(dobpdc)–*air* and MOF-74-Mg. The CO_2 loading (at 1 bar and 25°C) and the N_2 loading (at 0.95 bar and 77 K) are also reported.

	S_{BET} ($m^2\ g^{-1}$)	$S_{Lanmguir}$ ($m^2\ g^{-1}$)	V_{pores} ($cm^3\ g^{-1}$)	N_2@77K, 0.95 bar (mmol g^{-1})	CO_2@RT, 1 bar (mmol g^{-1})
Mg_2(dobpdc)–*act*[a]	2941	3895	1.47	44.9	6.4
Mg_2(dobpdc)–*sol*[a]	1761	2332	0.89	25.9	2.1
Mg_2(dobpdc)–*air*[a]	513	680	0.29	8.4	4.8
MOF-74-Mg[a,b]	1495	1905	0.68	19.6	8.0

[a]Standard range of pressure considered in the fit for the surface area evaluation: $0.05 < p/p_0 < 0.20$. V_{pores} evaluated at $p/p_0 = 0.95$. [b]Data from Ref. [4].

S6. IR spectra of CO_2 on Mg_2(dobpdc)–*act*, on Mg_2(dobpdc)–*sol* and Mg_2(dobpdc)–*air*.

The IR spectra of CO_2 reported in the 2500-2200 cm^{-1} range in Figure 3 in the main text are reported in Figure S7 extending the spectral region to 3900-650 cm^{-1}. A zoom view is reported on the spectral regions around the frequency corresponding to the CO_2 vibrational features: bending mode (680-620 cm^{-1}), CO_2 Fermi resonance (3800-3600 cm^{-1}) and CO_2 asymmetric stretching mode (2500-2200 cm^{-1}). It is interesting to notice that in the 3800-3600 cm^{-1} region framework overtones appear after MOF interaction with the CO_2 molecules, that are superimposed to the CO_2 Fermi resonance and then less appreciable in the spectra than for CO and N_2. These modes were observed upon gas dosage for all the adsorbates used in this study.

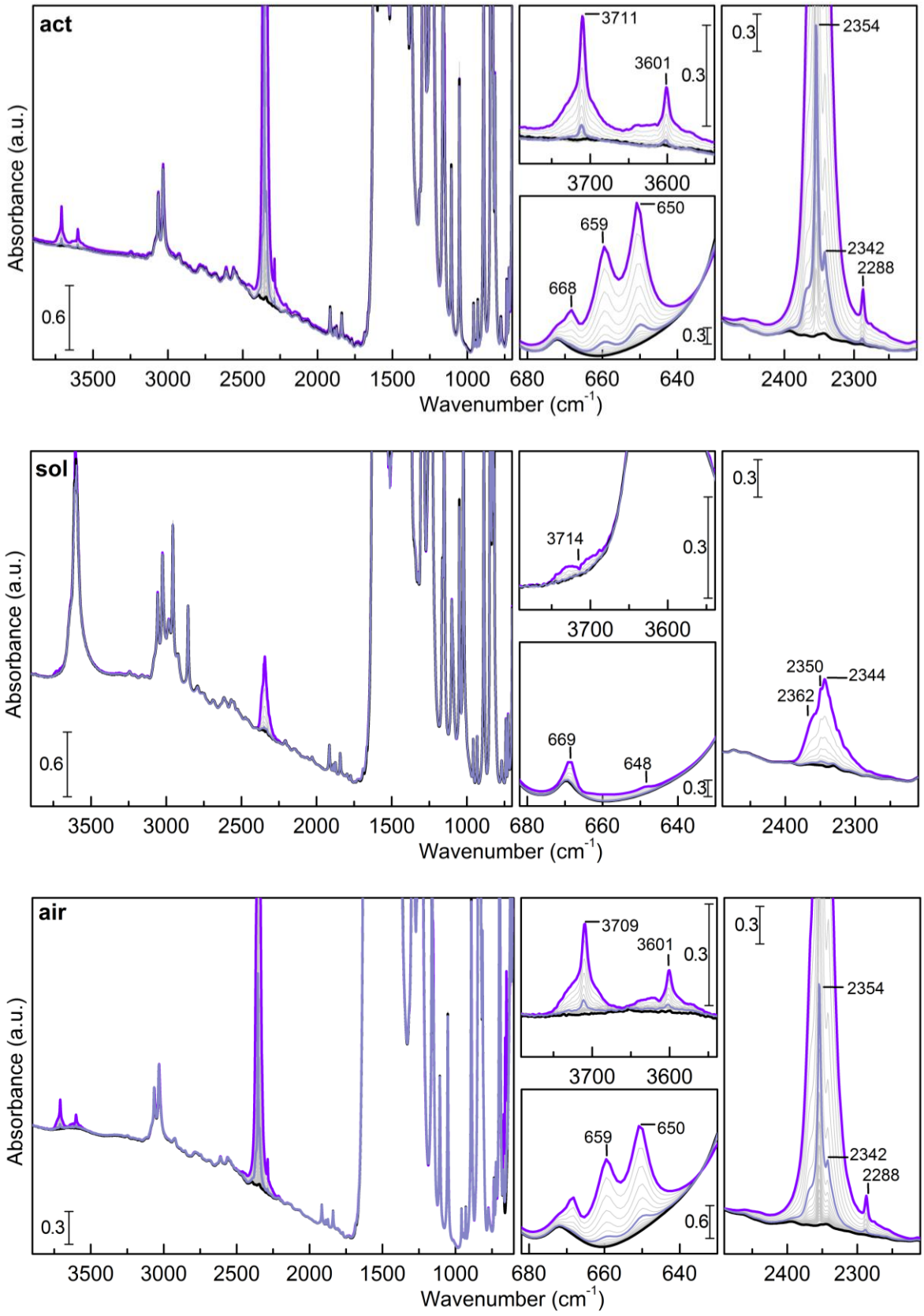
act
Absorbance (a.u.)
0.6
3711
3601
0.3
3700
3600
659
650
668
0.3
0.3
2354
2342
2288
3500
3000
2500
2000
1500
1000
680
660
640
2400
2300
Wavenumber (cm-1)
sol
Absorbance (a.u.)
0.6
3714
0.3
3700
3600
669
648
0.3
0.3
2350
2344
2362
3500
3000
2500
2000
1500
1000
680
660
640
2400
2300
Wavenumber (cm-1)
air
Absorbance (a.u.)
0.3
3709
3601
0.3
3700
3600
659
650
0.6
0.3
2354
2342
2288
3500
3000
2500
2000
1500
1000
680
660
640
2400
2300
Wavenumber (cm-1)

Figure S10. FTIR spectra of CO_2 adsorbed on (from top to bottom) Mg_2(dobpdc)–*act*, Mg_2(dobpdc)–*sol* and Mg_2(dobpdc)–*air* recorded at beam temperature. The spectra were obtained by increasing CO_2 equilibrium pressure from vacuum (black curve) to 1 mbar (light violet) and 44 mbar (violet curve). Light grey curves refer to intermediate coverage. The spectrum obtained after degassing overnight at beam temperature was coincident with the spectrum recorded initially in vacuum and then it was not reported. The four panels correspond to four different spectral regions (from left to right): 3900-650 cm^{-1} (the whole spectral region considered in the measurements), 3800-3600 cm^{-1} (Fermi resonance of the CO_2 molecules, water contaminants, frameworks overtone), 680-620 cm^{-1} (CO_2 bending frequency region), 2500-2200 cm^{-1} (CO_2 stretching region). a.u. = absorbance units.

S7. IR spectra of CO at 100 K on Mg_2(dobpdc)–*act*, Mg_2(dobpdc)–*sol* and Mg_2(dobpdc)–*air*.

The IR spectra of CO reported in the 2500-2200 cm^{-1} range in Figure 3 of the main text are reported in Figure S7 extending the spectral region to 3900-650 cm^{-1}. A zoom view is reported for the spectral regions corresponding to framework overtones (3800-3540 and 1975-1810 cm^{-1}) and CO stretching mode (2250-2020 cm^{-1}).

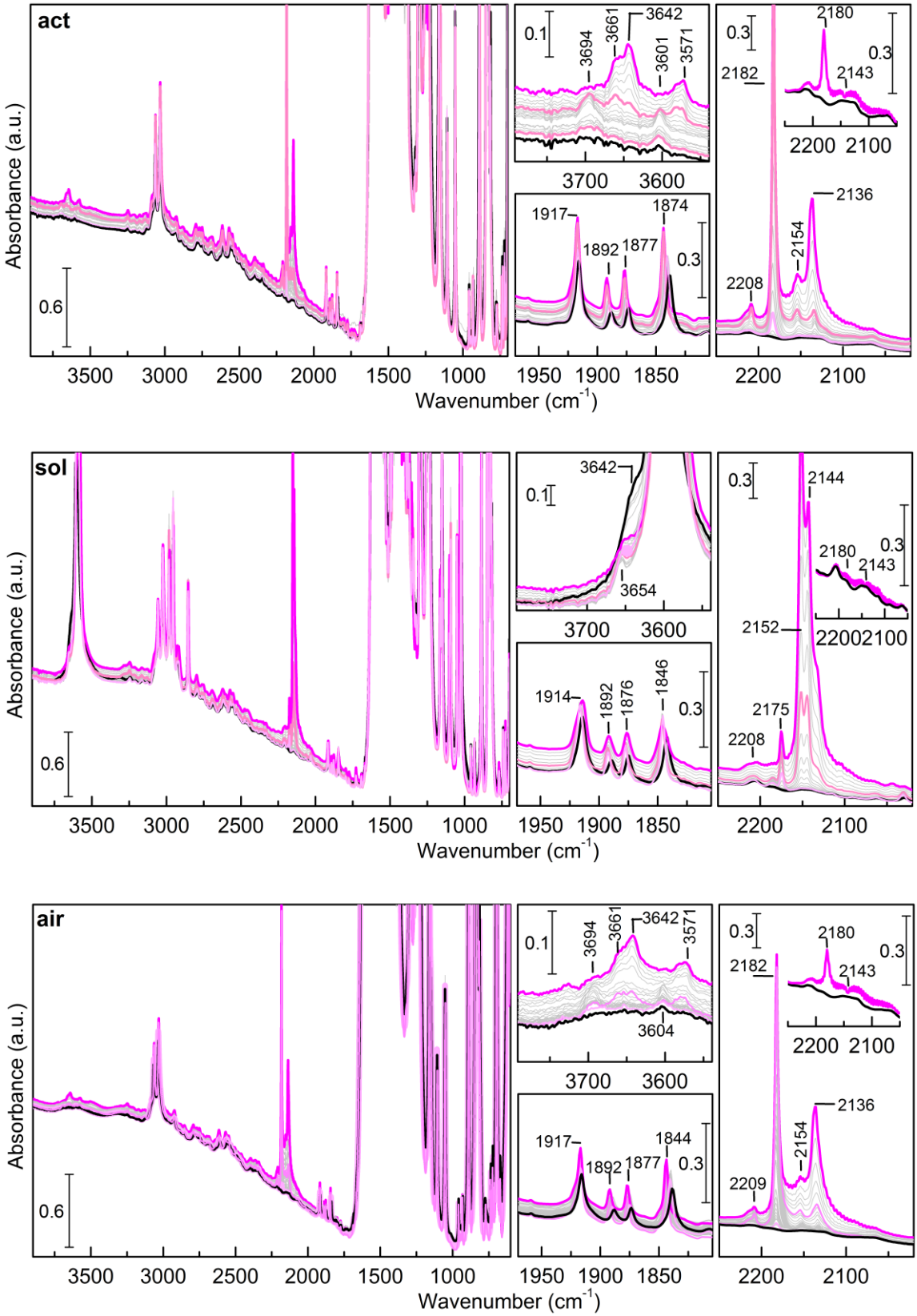
act
sol
air
Absorbance (a.u.)
Wavenumber (cm-1)
0.6
0.1
0.3
3694
3661
3642
3601
3571
3654
3604
1917
1892
1877
1874
1914
1876
1846
1844
2180
2143
2182
2200 2100
2136
2154
2208
2144
2152
2175
2209
3700 3600
3500 3000 2500 2000 1500 1000
1950 1900 1850
2200 2100

Figure S11. FTIR spectra of CO adsorbed on (from top to bottom) Mg_2(dobpdc)–*act*, Mg_2(dobpdc)–*sol* and Mg_2(dobpdc)–*air* recorded at 100 K. 44 mbar of CO were dosed at beam temperature on the sample (inset in the right panels) and then the temperature was decreased to 100 K. Once that equilibrium was reached, the spectra were recorded upon decreasing CO equilibrium pressure from 12 mbar (pink curve) to vacuum (black curve). Light grey curves refer to intermediate coverage besides two (at 1 and 0.01 mbar) that have been indicated with pink shades. The spectrum obtained after prolonged degassing was coincident with the spectrum recorded initially in vacuum and then it was not reported. The four panels correspond to four different spectral regions (from left to right): 3900-650 cm^{-1} (the whole spectral region considered in the measurements), 3800-3540 cm^{-1} (water contaminants, frameworks overtone), 1975-1810 cm^{-1} (framework overtones), 2250-2020 cm^{-1} (CO stretching region). The inset in the right panels reports the spectrum obtained at BT and 44 mbar of pressure. a.u. = absorbance units.

S8. IR spectra of N_2 at 100 K on Mg_2(dobpdc)–*act*, on Mg_2(dobpdc)–*sol* and Mg_2(dobpdc)–*air*.

The IR spectra of N_2 reported in the 2500-2200 cm^{-1} in Figure 3 in the main text are reported in Figure S7 extending the spectral region to 3900-650 cm^{-1}. A zoom view is shown on the spectral regions corresponding to frameworks overtone (3800-3540 and 1975-1810 cm^{-1}), and the N_2 stretching region (2400-2300 cm^{-1}).

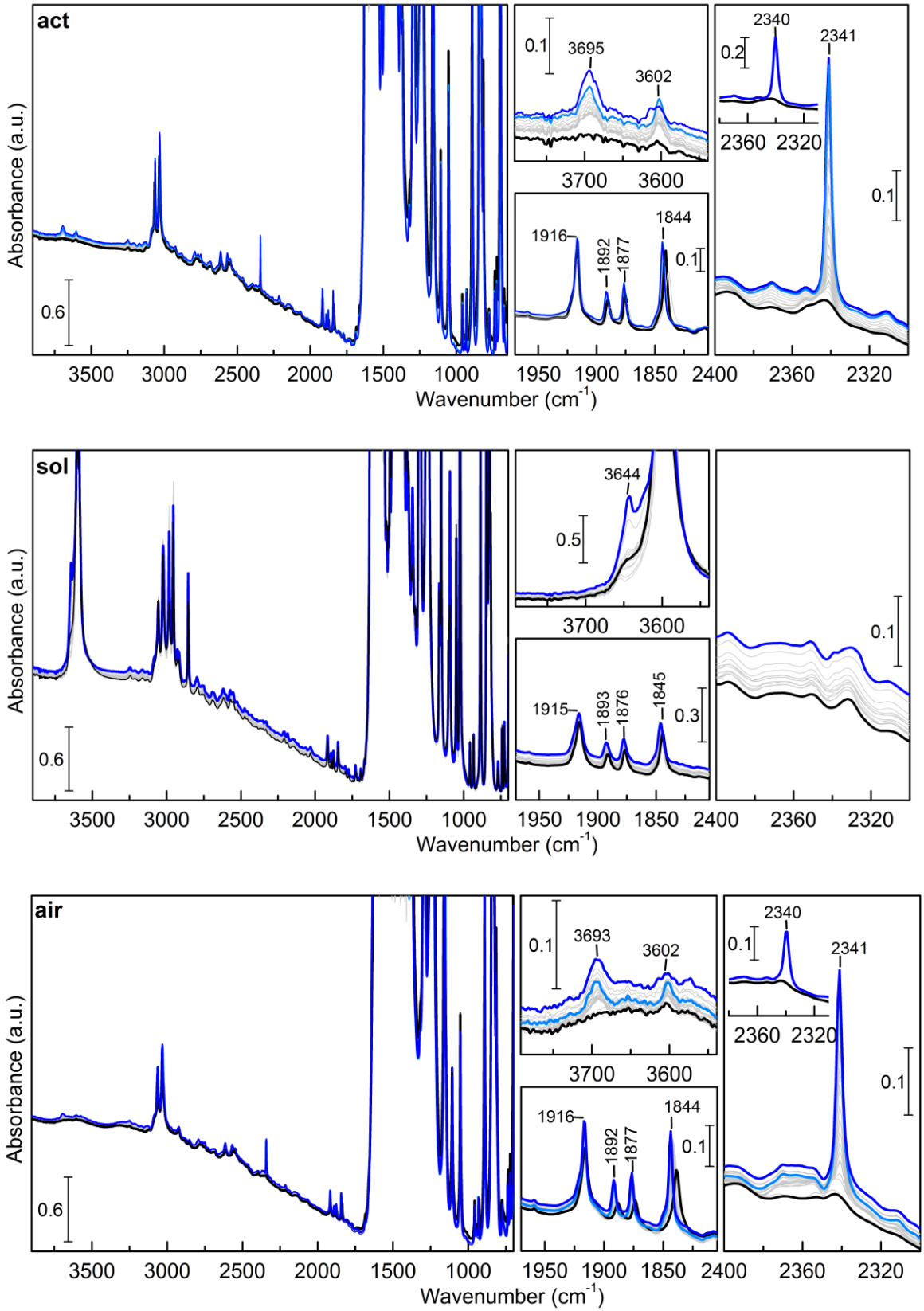
act
sol
air
Absorbance (a.u.)
Wavenumber (cm-1)
3695
3602
3644
3693
1916
1892
1877
1844
1915
1893
1876
1845
2340
2341
0.6
0.1
0.2
0.5
0.3
3500 3000 2500 2000 1500 1000
1950 1900 1850
2400 2360 2320
3700 3600
2360 2320

Figure S12. FTIR spectra of N_2 adsorbed on (from top to bottom) Mg_2(dobpdc)–*act*, Mg_2(dobpdc)–*sol* and Mg_2(dobpdc)–*air* recorded at 100 K. 44 mbar of N_2 were dosed at beam temperature on the sample (spectra reported in the insets of the rights panels) and then the temperature was decreased to 100 K. Once that equilibrium was reached, the spectra were recorded upon decreasing N_2 equilibrium pressure from 41 mbar (blue curve) to vacuum (black curve). Light grey curves refer to intermediate coverage besides the one recorded at 21 mbar (light blue curve). The spectrum obtained after prolonged degassing at beam temperature was coincident with the spectrum recorded initially in vacuum. The four panels correspond to four different spectral regions (from left to right): 3900-650 cm^{-1} (the whole spectral region considered in the measurements), 3800-3540 cm^{-1} (water contaminants, frameworks overtone), 1975-1810 cm^{-1} (framework overtones), 2400-2300 cm^{-1} (N_2 stretching region). The inset in the right panels reports the spectrum obtained at BT and 44 mbar of pressure. a.u. = absorbance units.

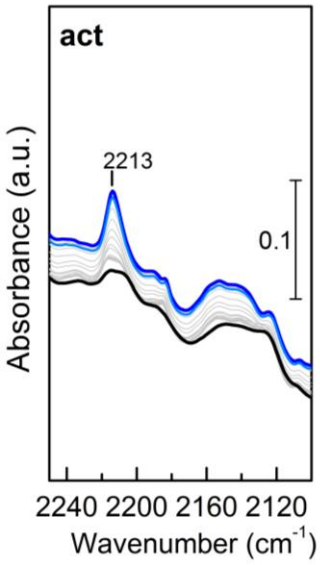

Figure S13. FTIR spectra of N_2 adsorbed on Mg_2(dobpdc)–*act* recorded at 100 K as in Figure S12 in the 2250-2100 cm^{-1} range. a.u. = absorbance units.

S9. Electrostatic potential maps of MOF-74-Mg and Mg_2(dobpdc)–*act*

In Figure S14, the structure of MOF-74-Mg is reported. The calculated electrostatic potential map of MOF-74-Mg and Mg_2(dobpdc) are compared in Figure S15 in the region around the Mg^{2+} sites. The two structures are indistinguishable for what concerns their electrostatic properties. The dark cyan region (largest positive value of the electrostatic potential) is observed in correspondence of the Mg^{2+} site. For what concerns the oxygen atoms, the five O around a Mg^{2+} are characterized by a different polarity. Two of them are from two different carboxylate units, each of them shared with another Mg ion (O_{COOs}). One oxygen is from one of the previous carboxylate units, but it is not shared with another Mg ion (O_{COOu}). The two remaining oxygens belong to the deprotonated OH group of two other linkers, each of them shared with another Mg ion (O_{OHs}). In one channel are present simultaneously 1 O_{OHs}, 2 O_{COOs}. 1 O_{COOu}. Only the two O_{OHs} and the O_{COOu} give a significant contribution to the ESP (red regions in the map) whereas the O_{COOs} are almost apolar (yellow-green regions).

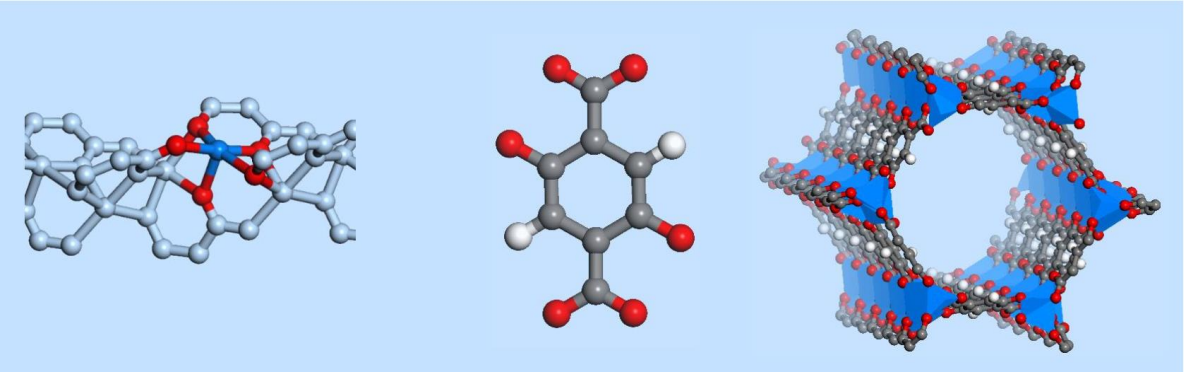

Figure S14. Structure of MOF-74-Mg. From left to right: inorganic node, organic linker and pore structure, as optimized at the B3-LYP-D*/TZVp level. The C atoms are reported in gray, H atoms in white, O in red, Mg in dark cyan.

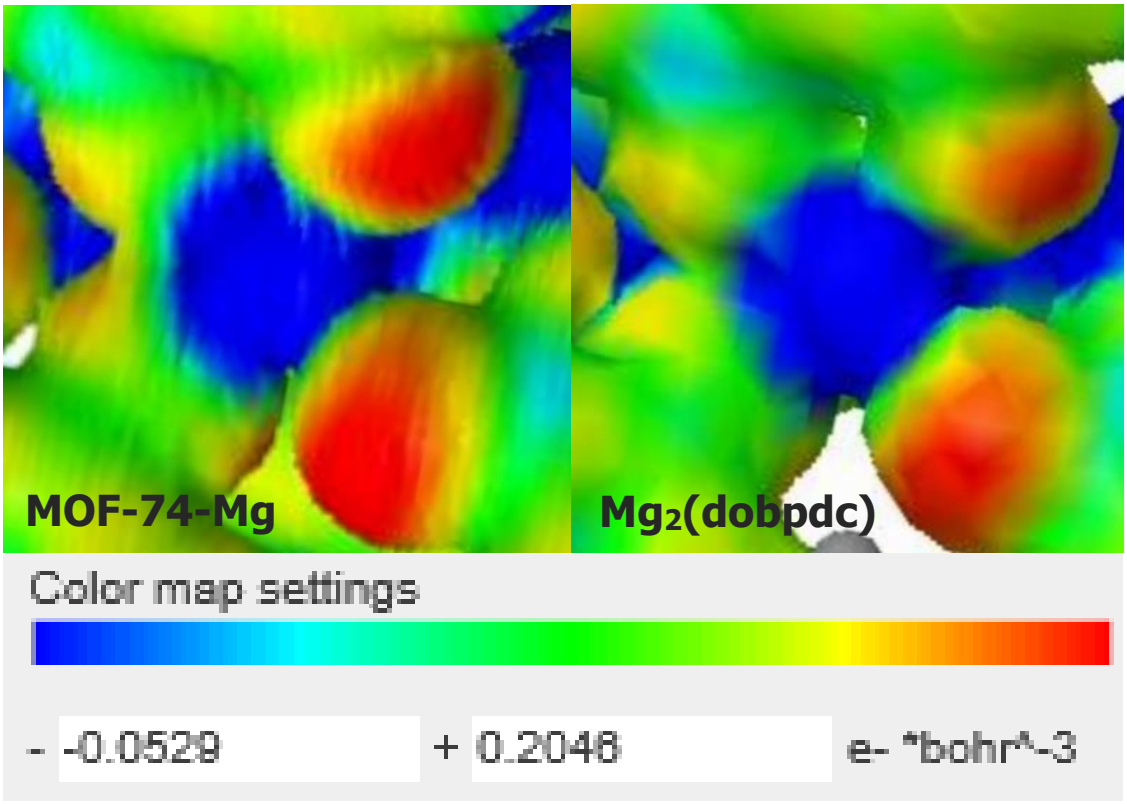

Figure S15. Electrostatic potential map of MOF-74-Mg and Mg_2(dobpdc)–*act* around the Mg^{2+} site (maps obtained by using the online version of the J-ICE program).[5]

S10. Instructions to visualize the calculated vibrational modes of Mg_2(dobpdc)–*act*, CO_2/ Mg_2(dobpdc)–*act*, CO/Mg_2(dobpdc)–*act* and N_2/Mg_2(dobpdc)–*act*.

The calculated normal modes for Mg_2(dobpdc)–*act*, CO_2/ Mg_2(dobpdc)–*act*, CO/Mg_2(dobpdc)–*act* and N_2/Mg_2(dobpdc)–*act* can be visualized by using the *.mol files present in the Supporting Information, readable with the Moldraw software (freeware upon registration at http://www.moldraw.unito.it/).

Open the program and then click on Read and select the *.mol file.

Then go in the menu:

Crystal

Make Box

Click on ok.

In this way you will visualize the crystal cell.

To visualize the normal modes select:

View

Normal modes

Select the frequency and then click on Animate. In order to better appreciate the movement, click on + or – of the Speed and Amplitude options.

To close the Frequency windows, click on Dismiss.

References

(1) Vitillo, J. G.; Bordiga, S. Increasing the Stability of Mg_2(dobpdc) Metal-Organic Framework in Air Through Solvent Removal, *Mater. Chem. Front.* **2017**, *1*, 444-448.

(2) Tan, K.; Zuluaga, S.; Gong, Q.; Canepa, P.; Wang, H.; Li, J.; Chabal, Y. J.; Thonhauser, T. Water Reaction Mechanism in Metal Organic Frameworks with Coordinatively Unsaturated Metal Ions: MOF-74, *Chem. Mater.* **2014**, *26*, 6886-6895.

(3) Mondloch, J. E.; Katz, M. J.; Planas, N.; Semrouni, D.; Gagliardi, L.; Hupp, J. T.; Farha, O. K. Are Zr6-based MOFs water stable? Linker hydrolysis vs. capillary-force-driven channel collapse, *Chem. Commun.* **2014**, *50*, 8944-8946.

(4) Caskey, S. R.; Wong-Foy, A. G.; Matzger, A. J. Dramatic Tuning of Carbon Dioxide Uptake via Metal Substitution in a Coordination Polymer with Cylindrical Pores, *J. Am. Chem. Soc.* **2008**, *130*, 10870-10871.
(5) Canepa, P.; Hanson, R. M.; Ugliengo, P.; Alfredsson, M. J-ICE: a new Jmol interface for handling and visualizing crystallographic and electronic properties, **2011**, *44*, 225-229.